Nonlin. Processes Geophys. Discuss., doi:10.5194/npg-2016-8, 2016
Manuscript under review for journal Nonlin. Processes Geophys.
Published: 25 January 2016

Nonlinear Processes in Geophysics
Discussions
Open Access

Ocean—atmosphere—wave characterization of a wind jet (Ebro shelf, NW Mediterranean Sea)

Manel Grifoll[1], Jorge Navarro[2], Elena Pallarès[1], Laura Ràfols[1,3], Manuel Espino[1] and Ana Palomares[2]

[1]{LIM/UPC (BarcelonaTech), Barcelona, Spain}

[2]{CIEMAT, Madrid, Spain}

[3]{Meteocat, Barcelona, Spain}

Correspondence to: M. Grifoll (manel.grifoll@upc.edu)

Abstract

In this contribution the wind jet dynamics in the northern margin of the Ebro River shelf (NW Mediterranean Sea) are investigated using coupled numerical models. The study area is characterized by persistent and energetic offshore winds during autumn and winter. During these seasons, a seaward wind jet usually develops in a 50km wide band offshore. The COAWST (Coupled Ocean—Atmosphere—Wave—Sediment Transport) modelling system was implemented in the region with a set of downscaling meshes to obtain high-resolution meteo-oceanographic outputs. Wind, wave and water current were compared with in situ observations and remote-sensing-derived products with an acceptable level of agreement. Focused on an intense offshore wind event, the modelled wind jet appears in a limited area offshore with a strong spatial variability. The wave climate during the wind jet is characterized by the developing of bimodal directional spectra, and the ocean circulation tends to present well-defined two-layer flow in the shallower region (i.e. inner shelf). The outer shelf tends to be dominated by mesoscale dynamics such as the slope current. Despite the limited fetch length, ocean bottom roughness considering sea state (wave-atmosphere coupling) modifies to a small extent the wind and significant wave height under severe cross-shelf wind events. However, the coupling effect in the wind resource assessment may be relevant due to the cubic relation between the wind intensity and power.

Keywords: wind jet, COAWST, ocean—atmosphere coupling, wind power assessment

1 Introduction

Coastal areas are often characterized by highly variable and heterogeneous wind, wave and current conditions, which make the numerical prediction of the meteo-oceanographic processes difficult. For instance, wind jets induced by orographic effects present strong spatial wind field variability due to the orographic characteristics (e.g. Shimada and Kawamura, 2006; Zhai and Bower, 2013). Due to the persistence in wind intensity and direction, these are regions exposed to the installation of offshore wind farms (Nunalee and Basu, 2013), and the resultant offshore winds decisively influence the exchange of water mass and material along the shelf/slope (Jordà et al., 2005; Barton et al., 2009). Instead of the relatively limited fetch in the wind jet region, the wave height can be relevant, interacting with bimodal features (Shimada and Kawamura, 2006). In this sense, several contributions have highlighted the influence of variable wind conditions in relatively small-scale areas (such as wind jet), influencing wind—wave generation (Shimada and Kawamura, 2006; Bolaños et al., 2007; Alomar et al., 2014) or modifying ocean circulation patterns (Csanady, 1980; Zhai and Bower, 2013; Schaeffer et al. 2011; Klaić et al., 2011).

In coastal zones the air—sea momentum transfer presents high complexity due to the dependence of wind intensity on sea bottom roughness. The relevance of the atmospheric bottom roughness increasing due to waves has been investigated in recent years (Janssen, 1989; Janssen and Viterbo, 1996; Lionello et al.1998; Taylor and Yelland, 2001; Oost et al., 2002; Drennan et al., 2003). In this sense, advanced computational tools have allowed to the feedback of meteo-oceanographic momentum and heat transfer to be addressed numerically (Warner et al., 2010; Zambon et al., 2014). Warner et al. (2010) developed a fully coupled numerical system (COAWST: Coupled Ocean—Atmosphere—Wave—Sediment Transport) to investigate the impact of storms on coastal systems. Using COAWST, Olabarrieta et al. (2012) and Renault et al. (2012) proved numerically that the wave-induced ocean bottom roughness is a key parameter in the air—sea momentum transfer. Under severe storm conditions (hurricanes and cyclones), this parameter influences the spatial and temporal evolution of the meteo-oceanographic variables. Other recent examples that use a fully numerical model to investigate the air—sea interaction and its effect on oceanographic processes are found in Nelson and He (2012) and Drews (2013).

The case of the Ebro River shelf (NW Mediterranean Sea; see Figure 1) is characterized by strong, dry and usually cold wind that blows from the north-west through the Ebro valley, induced by the lee of the Pyrenees mountains. The westerly wind, greatly affected by the orography, is channelized into a limited band, forming a wind jet (Jansà, 1985; Spanish Ministry of Energy, 2004). The synoptic situation is related to an anticyclone in the Bay of Biscay and a low-pressure area in the Mediterranean Sea (Riosalido et al., 1986; Font, 1990; Martín-Vide, 2005; Cerralbo et al., 2015). Offshore wind is more usual and intense during autumn and winter, when larger atmospheric pressure gradients take place and cause stronger winds with advection of cold air, but a small atmospheric pressure difference along the Ebro valley is sufficient to initiate wind during any season (Riosalido et al., 1986; Cerralbo et al., 2015).

The objective of this contribution is to describe the meteo-oceanographic processes associated with a wind jet developing at the northern margin of the Ebro River shelf. This work provides insight into wind jet in a complex area from an orographic point of view, such as the Ebro delta shelf, describing the main wind, wave and current patterns and evaluating the feedback in the air—sea momentum transfer in terms of wave-induced ocean bottom roughness. After the introduction (Section 1), in Section 2 (Methods) we describe the study area, the COAWST model implementation and the wind jet event selected to investigate in detail the meteo-oceanographic dynamics. Then, in Results (Section 3) we show the most relevant meteo-oceanographic processes observed and a detailed skill assessment of the fields modelled, comparing with a set of available data (i.e. in situ observations and remote-sensing products). Also, the feedback in the air—sea momentum transfer in terms of wave-induced ocean bottom roughness is investigated with a set of simulations testing different air—sea momentum transfer formulations. Afterwards, we discuss (Section 4) the relevance and particularities of the dynamics of the wind jet area in terms of waves, winds and currents, comparing with previous investigations. The implications of the wind—wave coupling in terms of the wind resource assessment are highlighted. We close with the conclusions (Section 5).

2 Methods

2.1 Study area and observations

The meteorological patterns over the NW Mediterranean Sea exhibit sharp gradients associated with the topographic control on synoptic fluxes (Jansà, 1985; Martin-Vide and Olcina, 2001). Regional wind analysis reveals strong and persistent cross-shelf winds. A channelization effect associated with the Ebro valley triggers north-westerly winds (called "Mestral"), resulting in a wind jet. Previous studies based on long-term wind measurements in the proximity of the region showed that winds have a persistent seasonal pattern (Font, 1990; Cerralbo et al., 2015; Grifoll et al., 2015). During winter and autumn, a dominant north-westerly component caused by wind channelization was observed. For instance, recent wind measurements revealed that cross-shelf winds were observed more than 60 % of the time during these seasons (Grifoll et al., 2015). In this period, the energy is concentrated in the low frequencies associated with synoptic scales (periods of 2—5 days, corresponding with the passage of weather systems). However, the warmer period (spring and summer) is characterized by high variability with a dominance of south-westerly winds. This means that during spring and summer the relative contribution of the daily components (breezes) to the variability increases with respect to the synoptic winds (Font, 1990; Cerralbo et al., 2015). The warmer seasons are less energetic than the cold seasons in terms of wind intensity.

The Ebro River delta is located immediately to the south of the wind jet region, and the average annual river discharge ranges between 300 and 600m^3·s^{-1}. The curvature of the bay partially shelters it from southerly waves. Regional wave climate in this area is characterized by south-east and east sectors, the latter being the most energetic due to the largest fetches (Bolaños et al., 2007).

Oceanographic investigations in the Ebro River region were focused primarily on the outer shelf and slope dynamics of the southern margin (Font, 1990; Palanques et al., 2002; Salat et al., 2002; Jordà, 2005) with relevant eddy activity (Redondo et al., 2013). The circulation in these regions is dominated by the inertial band, with a relevant signal of the slope current associated at the regional Northern Current (Jordà, 2005). Observational analyses have revealed that the inner and mid-shelf (less than 50m water depth) dynamics in the Ebro shelf are characterized by a strong influence of the frictional component of the flow (Jordà, 2005, Grifoll et., 2015). Furthermore, the regional response to wind jets is not clear due to the complex bathymetry and the spatial variability of the wind jet. Durand et al. (2002) and Mestres et al. (2003) showed that the effects of the salinity river plume are important only near the river mouth (order of 10km offshore from the river mouth).

As a part of large effort to collect physical data and implement numerical tools for the development of offshore wind energy, a buoy was moored in the northern margin of the Ebro shelf where the wind jet develops (see Figure 1). The buoy was moored 3.1km from the coast at 43.5m bottom depth, measuring wind, waves and water currents for one year. A TRIAXYS directional wave sensor mounted on the moored buoy was used to record statistical wave spectra parameters. Wind speed and direction were measured at 4m height every 10min using an ultrasonic wind sensor (Gill Instruments) for one year (November 2011 to November 2012). Water currents were measured with a SonTek acoustic Doppler currentmeter profiler (ADCP) at 500kHz every hour using 20 vertical layers (layer depth was 2m). The mooring period covered more than one year (from November 2011 to December 2012).

Additionally, satellite-measured winds were used for the numerical model validation. Sea wind intensity and direction were obtained from the National Climatic Data Center (NCDC-NOAA, http://www.ncdc.noaa.gov/oa/rsad/air-sea/seawinds.html). This product is the result of a spatial and temporal interpolation of the data received from the different satellites passing through the study area during a time interval, and it has 6h time resolution and 15km spatial resolution.

2.2 Numerical model and meshes

The COAWST modelling system (Warner et al., 2010) was used in this study. COWAST relies on the 3-D ocean modelling ROMS (Regional Ocean Modeling System; see Haidvogel et al., 2000), the phase-averaged wave model SWAN (Simulating WAaves Nearshore; see Booij et al., 1999), the non-hydrostatic meteorological model WRF (Weather Research and Forecasting; Skamarock et al., 2005) and the sediment transport module CSTMS (Community Sediment Transport Modeling System; Warner et al., 2010). The ocean model ROMS is a free-surface, terrain-following numerical model which resolves the three-dimensional Reynolds-averaged Navier—Stokes (RANS) equations using hydrostatic and Boussinesq approximation. The WRF model (Advanced Research WRF version) is a non-hydrostatic, quasi-compressible atmospheric model with boundary layer physics schemes and a variety of physical parameterizations of sub-grid scale processes for predicting meso- and microscales of motion. The SWAN model solves the wave action balance equation simulating wind generation and propagation in deep and coastal waters. The modelling system COAWST includes the coupler Model Coupling Toolkit (MCT; Jacob et al., 2005) for the transmission and transformation of the physical variables using a parallel computing approach. The COAWST system also allows for the exchange of data fields on different grids using the Spherical Remapping Interpolation Package (SCRIP; Jones, 1998) to compute the interpolation weights. The nesting strategy consists of a set of different downscaling meshes (Figure 1c and Table 1). The ocean—atmospheric—wave online coupling was implemented in the finer domain (mesh O4 for the wave and circulation model, and mesh M4 for the meteorological model) where the scale of the coupling process due to cross-shelf winds may be more evident in the results.

The largest wave domain (mesh O1) covers the western Mediterranean Sea, which is considered enough to capture the wave generation in the study area. The SWAN model implementation used amends the underestimation in the wave growth rates reported by Alomar et al. (2014) and Rogers et al. (2003) in a low- and medium-frequency energy spectrum. The measure adopted was introduced by Pallares et al. (2014) and consists in modifying the whitecapping dissipation term (see Appendix 1).

Nonlin. Processes Geophys. Discuss., doi:10.5194/npg-2016-8, 2016
Manuscript under review for journal Nonlin. Processes Geophys.
Published: 25 January 2016

Nonlinear Processes in Geophysics
Discussions
Open Access

The largest water circulation domain (mesh O3) is nested into the daily MyOcean-MEDSEA product (Tonani et al., 2009), with a horizontal resolution of 1/16ºx1/16º and 72 unevenly spaced vertical levels, in order to provide suitable boundary conditions for the oceanographic variables in terms of water velocity, sea level, temperature and salinity. The 3D ocean model implementation (ROMS) includes a generic length scale turbulent mixing scheme (Umlauf and Burchard, 2003), with coefficients selected to parameterize the K-epsilon scheme (Rodi, 1987) and fourth-order biharmonic Laplacian viscosity and mixing terms on geopotential surfaces for velocity and tracers, respectively, both with constant coefficients of $0.5m^4s^{-2}$. The bottom boundary layer was parameterized using a log profile with bottom roughness equal to 0.005m.

The atmospheric model is nested into the ECMWF ERA-Interim reanalysis product considering four downscaling meshes – M1, M2, M3 and M4 with resolutions of 27km, 9km, 3km and 1km, respectively – to obtain suitable grid resolution for the complex orography of the region (see Figure 1). The WRF implementation uses a Mellor—Yamada—Nakanishi—Niino (MYNN) level 2.5 planetary boundary layer scheme.

2.3 Episode description and numerical sensitivity test

As we noted in the introduction, the air—sea momentum transfer presents high complexity due to the relation of wave characteristics and the sea bottom roughness, which in turns affect the wind field. In order to investigate the air—sea momentum transfer in the wind jet, a set of simulations have been designed applying different air—sea momentum transfer formulations included in the COAWST modelling system. The sensitivity tests pursue an evaluation of the "coupling" effects on two principal variables involved in the air—sea momentum transfer: wind intensity (W) and significant wave height (H_s). In this sense three different formulations have been tested (see Appendix 2), which consider the modification of the atmospheric bottom roughness due to the waves. In consequence, we compare directly the "coupled" results with an "uncoupled" simulation where the bottom roughness length is only a function of the wind stress. The sensitivity tests are as follows: CHK for the simulation considering the bottom roughness as a function of the wind stress (uncoupled with the wave sea state) using the Charnok coefficient equal to 0.016 (typical value for rapidly seas), T—Y simulation considering the Taylor and Yelland formulation (Taylor and Yelland, 2001), DRE using the Drennan formulation proposed by Drennan et al. (2003) and OOST simulation considering the formulation introduced by Oost et al. (2002). Two numerical points are chosen to compare

Nonlin. Processes Geophys. Discuss., doi:10.5194/npg-2016-8, 2016
Manuscript under review for journal Nonlin. Processes Geophys.
Published: 25 January 2016

the results for the sensitivity test simulations. One point is near the buoy's moored position (where the numerical results are also compared with the measurements). The second point is located 30km offshore of the measurement point (see control point in Figure 1). This point has been chosen in order to capture the wave growth due to cross-shelf winds and evaluate properly the coupling—uncoupling differences.

We select a cross-shelf wind event in order to characterize in detail the meteo-oceanographic dynamics of the wind jet. The episode selected for the sensitivity tests lasted from the 19th of March 2012 to the 23rd of March 2012. The synoptic situation during the selected episode corresponds to a typical offshore wind event induced by atmospheric pressure differences (see Figure 2). A high-atmospheric-pressure area is centred over the North Atlantic Ocean, with the anticyclonic edge affecting part of the Iberian Peninsula. The low pressure is located in the centre of Europe. In this situation the cross-shore winds in the Ebro delta zone are intensified. The sequence of wind field modelled in the Catalan coast mesh during the wind jet period is characterized by a rise of wind intensity during the 20th and 21st of May, leading to a wind jet in the northern margin of the Ebro delta (see daily-averaged wind intensity in Figure 3). Then, the cross-shore winds remains strong during the 22nd of May, decreasing during the 23rd of May 2012.

3 Results

3.1 Description of meteo-oceanographic processes and skill assessment

Modelled winds during the simulation period reproduce the main wind directions previously reported in the study area. Offshore wind prevails throughout the year, intercalated with southerly winds during spring and summer (i.e. sea breeze). The adjustment of the wind time series into a Weibull distribution is used to evaluate the statistical inter-comparison between wind observations (measured from the buoy and satellite) and the 3km WRF model results (mesh M3). Blended Sea Winds were used from the NCDC-NOAS SeaWinds project which contain 6-hourly globally gridded, high-resolution ocean surface vector winds and wind stresses on a global 0.25° grid. Figure 4 shows the Weibull distributions considering the wind intensity time series. Also the global model (i.e. ECMWF) used for WRF model downscaling is included. The results show that the numerical simulation presents better agreement with the wind measurements than the global model and the gridded satellite wind estimations. Although the global wind model assimilates the satellite information, the Weibull distribution

Nonlin. Processes Geophys. Discuss., doi:10.5194/npg-2016-8, 2016
Manuscript under review for journal Nonlin. Processes Geophys.
Published: 25 January 2016

of the high-resolution model presents a better level of agreement than the observations. A snapshot of the SeaWinds product was compared with the numerical outputs in Figure 5. Wind patterns from both products present a significant level of agreement in both components assuming the coarser resolution of the SeaWinds. Additional verification is presented in Table 2 using model—observation statistics in terms of wind intensity for the whole year of 2012. In summary, modelled winds show an acceptable level of agreement with the observations.

In Figure 6, time series comparing the results obtained from the coupled SWAN model (mesh O3) and the buoy measurements (see position in Figure 1) are shown. The time series comparison corresponds to the significant wave height (H_s), the mean wave period (Tm_{01}) and the mean wave direction (θ_w). In general, the model reproduces the observations in terms of mean behaviour and variability. Table 2 presents the error statistics for the whole year for mesh O3 in terms of H_s and Tm_{01}.

Figure 7a show a snapshoot of the waves' directional spectra during the wind jet period selected at the measuring point; the results reveal the tendency to develop bimodal directional spectra due to the co-existence of sea and swell waves. Directional spectra presents a peak around -50º mean wave direction associated with the growing wave due to the wind jet and another peak around 150º associated with the swell. Due to the limited fetch, larger wave frequencies (smaller wave period) are obtained for the -50º wave direction peak than for the 150º wave direction peak. In Figure 7b the directional spectra for a period without wind jet are also shown for comparison. In this case, unimodal wave spectra is obtained. In summary, the high-resolution mesh (O4) is able to capture the bimodal spectra during wind jet. Unfortunately, only the statistical spectra parameters were recorded in the buoy measurements, and full spectra comparison is not possible.

The water circulation observed at the buoy is characterized by an alignment of the flow following the isobaths. The principal component analysis of the flow for the observed depth-averaged currents reveals an angle similar to the coastline orientation (~26º). As the cross-shelf flow is limited by the coastline, the variability in this direction is smaller than in along-shelf direction: standard deviation is $2.3 cm \cdot s^{-1}$ in cross-shelf direction versus $7.4 cm \cdot s^{-1}$ in along-shelf direction. However, the water circulation during the wind jet events shows a different pattern. During these events, the cross-shelf flow variability increases ($3.8 cm \cdot s^{-1}$ for the wind jet event selected), with either two-layer flow or an offshore flow in the whole water column. As an example of water current response during wind jet event, the along-shelf and

Nonlin. Processes Geophys. Discuss., doi:10.5194/npg-2016-8, 2016
Manuscript under review for journal Nonlin. Processes Geophys.
Published: 25 January 2016

Nonlinear Processes in Geophysics Discussions

cross-shelf velocities are shown in Figure 8 for May 2012 at the observational point (negative values mean south-westward and positive north-eastward). The surface currents in the cross-shelf direction intensify, causing an eventual two-layer flow during the peak of the wind intensity (21st of May). When the wind jet calms down, the cross-shelf velocities are small while the along-shelf flow intensity is larger than that of the cross-shelf. The along-shelf current observed during wind jet events tends to reverse from south-westward to north-eastward.

The skill assessment of the numerical results in terms of current (water velocity) was carried out following a similar scheme to the one used for winds and waves. The numerical model validation with ADCP observations shows an acceptable level of agreement according to the comparison for the wind jet event. For instance, Figure 8 shows a noticeable agreement between the observed and modelled currents in the water column for both along- and cross-shelf components. In addition, Table 2 presents the error statistics for the depth-averaged velocity measurements compared with the numerical model results for the wind jet event.

The spatial water circulation modelled during the wind jet event (21st of May) is shown in Figure 9 for two different depths: sub-surface (2m water depth) and intermediate (50m water depth). Depth-averaged velocities are also presented (Figure 9c). The surface current modelled at 1km (mesh O3) and 250m (mesh O4) grid resolution presents a relatively homogeneous offshore direction qualitatively that is well correlated with the spatial distribution of the wind intensity. In this case, the surface current is seldom affected by the topographic features such as the Ebro delta. At deeper layers the flow direction turns onshore, resulting in a two-layer flow in which the current intensity is lower than that of the surface layer. The depth-averaged flow is small due to the balance between the sheared two-layer flow; however, a flow component slightly appears that is aligned with the isobaths in the deeper areas of the continental shelf. Related to that, a clear signal of the slope current is observed in the results at -50m and depth-averaged currents.

3.2 Ocean bottom roughness numerical experiments

The wind intensity and the significant wave height during the selected wind jet event for the four simulations are shown in Figure 10 (for the control and observational points shown in Figure 1). Comparing the numerical results and the observations (Figure 10.a and 10.b), all the numerical simulations reproduces the wind intensity and the significant wave height with

Nonlin. Processes Geophys. Discuss., doi:10.5194/npg-2016-8, 2016
Manuscript under review for journal Nonlin. Processes Geophys.
Published: 25 January 2016

Nonlinear Processes in Geophysics
Open Access
Discussions

a similar level of agreement. The uncoupled (CHK) and coupled simulations (e.g. T-Y, OOST and DRE) only present differences in the numerical outputs during the jointly occurrence of strong winds and wave peaks in the control point. Waves and wind intensity numerical results at the observational point do not presents significant changes among the four simulations due to the limited fetch conditions which means lower significant wave height in comparison to control point. During the calm period (at beginning and end of the wind jet event) the differences among the four simulations are not appreciable. Comparing the error statistics for the observational point among the three coupled numerical simulations we cannot assure which formulation ensures a better skill assessment (Table 3). Although OOST sensitivity case presents better agreement at the observational point, the relative size of the wind intensity and significant wave height limits the conclusions for the wind-jet event. At control point the magnitude of the wind intensity and the significant wave height is larger for the uncoupled simulation (CHK) in comparison to coupled simulations. Maximum differences of 3 $m \cdot s^{-1}$ in wind intensity and 0.3 m in significant wave height are obtained if we compare OOST and CHK simulations.

4 Discussion

The shape of the wind jet modelled is benefited by the high resolution meshes used in our investigation. According to our results, the wind jet approximately covers an area of 50 km width offshore. This area is in agreement with the wind intensity atlas provided by the Spanish Ministry of Energy (see Figure 11) obtained from a long-term reanalysis. In this sense, high-resolution meshes used in this investigations (i.e. 1 km and 3 km grid resolution) are suitable for an accurate wind jet modelling. As it was pointed out by Alomar et al. (2014) and Cerralbo et al. (2015), the relevance of winds in the ocean response in terms of waves and currents justifies the high-resolution in the modelling investigations in Ebre Delta region.

Our results have shown an acceptable representation of the bimodal structure of the significant wave height and support the conclusions highlighted by Alomar et al (2014), whose note that a high spatial resolution of wind field is required to represent acceptable numerical wave field in a very limited fetch conditions. The occurrence of bimodal wave features may also have different implications: the first one is that, because of the spatial resolution, the local northwesterly wind that produced the second peak of spectra may not have been detected in previous investigations (Bolaños et al., 2005, 2006; Sánchez-Arcilla et al., 2008; Alomar et al., 2014). The second implication is related to the momentum transfer,

Nonlin. Processes Geophys. Discuss., doi:10.5194/npg-2016-8, 2016
Manuscript under review for journal Nonlin. Processes Geophys.
Published: 25 January 2016

Nonlinear Processes in Geophysics
Open Access
Discussions

where several authors have highlighted that under mixed wave-train conditions the drag coefficient may increase appreciably (Sánchez-Arcilla et al., 2008). Also, the wave modelling deserves a particular comment related to the good fitting of wave results thanks to the modification of a parameter relative to whitecapping dissipation (Pallarès et al., 2014). Statistical errors were reduced significantly due to the young sea developed in the wind jet region in comparison to previous investigations (Bolaños et al., 2007; Sánchez-Arcilla et al., 2008). In particular, smaller root mean square errors were obtained in the mean wave period variable, which presented a large uncertainty (Bolaños et al., 2007; Sánchez-Arcilla et al., 2008; Alomar et al., 2014).

As we noted in the Results section, the water circulation pattern showed differential behaviour for the long-term water circulation in comparison to the wind jet event. For the long-term circulation and in the shallow region, the frictional response prevails, with the along-shelf flow variability being larger than the cross-shelf flow, similar to other investigations in the inner and mid-shelf (see review in Lentz and Fewings, 2012). However, a different picture occurs during the wind jet event. In this case a characteristic surface current is high correlated to the offshore wind. According to the numerical outputs and in situ observations shown in Figure 8, a deeper onshore flow, opposing the surface layer flow offshore, is developed. This flow is relatively weak due to the prevalence of the along-shelf component which increases offshore. These circulation patterns are consistent with other investigations (e.g. Horwitz and Lentz, 2014; Fewings et al., 2008; Dzowonkowski et al., 2011) where a well-developed two-layer flow due to intense cross-shelf winds tends to occur when the turbulent layers overlap (water depth in the inner shelf is of the order of metres to tens of metres according to Lentz and Fewings, 2012). In the mid- and outer shelf, the flow tends to be oriented in the along-shelf direction due to the prevalence of the regional response to the wind jet and the slope current. In this sense, the frictional adjustment time due to the wind (inversely proportional to the depth) varies in the continental shelf section and may be of the order of days in the mid-/outer shelf (Csanady, 1982). In consequence, the expected response at deeper layers will also be dependent on processes acting at larger scales than wind jet (i.e., baroclinic forcing, mesoscale activity etc.) such as the slope current signal observed at 30m water depth and depth-averaged currents (Figure 9b and Figure 9c, respectively). The along-shelf flow in the inner shelf is presumably influenced by the regional response to the wind jet at the stratification in the water column and the barotropic pressure gradient adjustment due the variability of the spatial wind variability. These factors play an important role in the resultant

Nonlin. Processes Geophys. Discuss., doi:10.5194/npg-2016-8, 2016
Manuscript under review for journal Nonlin. Processes Geophys.
Published: 25 January 2016

Nonlinear Processes in Geophysics
Open Access
Discussions

water circulation pattern and its variability deserves additional numerical efforts and extended local wind and sea level information. For instance, Oey et al. (2004) and Liu and Weisberg (2012) include extended measurements to investigate the water circulation' response to spatial wind and the particular role of the barotropic pressure gradients. Finally, it is worth noting that the interaction between offshore winds and regional circulation was filtered in previous investigations in the zone region (Font, 1990; Salat et al., 2002; Jordà, 2005).

Several investigations have found the importance of the sea state in the impact on the air—sea momentum flux; in particular the calculations based on the Charnock constant underestimated the air—sea momentum transfer (e.g. Janssen and Viterbo, 1996; Drennan et al., 2003) which can be significant under mixed seas (Sanchez-Arcilla et al., 2008). In the northern margin of the Ebro delta and during the wind jet, no relevant differences were found when comparing the significant wave period and the wind intensity between numerical model and observations for the observational point. During calm periods, the averaged conditions prevail over energetic events, so the feedback of the air—sea momentum does not show significant differences. The detailed analysis of the 21st -22nd of May event showed significant differences between the coupled and uncoupled cases for significant wave height and wind intensity offshore of the wind jet (e.g. control “offshore” point). When we compare the coupling numerical results (i.e. T—Y, OOST and DRE) versus CHK results, we observe that the wind intensity at the control point is affected significantly by the sea state during the energetic event. For the coupling simulations the wind intensity is reduced due to wave-induced ocean bottom roughness increasing. This behaviour is consistent with other coupling atmosphere—ocean investigations under a high level of meteorological energy (e.g. Olabarrieta et al., 2012). In parallel, the wave field is modified by the feedback between wave and wind stress. During the energetic wind event selected, H_s is lower in comparison to the uncoupled case (CHK), consistent with other numerical experiments (Webber, 1993; Warner et al., 2010; Olabarrieta et al., 2012) and observational investigations (Yelland et al. 1998; Edson, 2008) which found that the momentum flux is underestimated using the Charnock constant parameter.

Differences in the primitive variables between the coupled and uncoupled simulations during particular energetic events are relatively small in terms of wind intensity and significant wave height. Furthermore, the assessment of the wind energy resource is relevant in this region with a high potential for wind farm installation due to the large and persistent wind intensity and

Nonlin. Processes Geophys. Discuss., doi:10.5194/npg-2016-8, 2016
Manuscript under review for journal Nonlin. Processes Geophys.
Published: 25 January 2016

Nonlinear Processes in Geophysics
Open Access
Discussions

the relatively large spatial extension of the continental shelf. A simple way to estimate turbine power from wind intensity is based on the idealized machine of blade diameter (D) being equal to 100m (Manwell et al., 2011):

$$P=\rho(2/3D)^2W^3 \quad . \qquad (1)$$

Wind intensity (W) simulations are taken at 10m height, so a log-law-based conversion is used to obtain wind values at 80m (typical value of turbine hubs). With the converted values of the numerical simulations, we estimate the idealized wind power for the period 21st–22nd of May 2012 at the control point. The power using the CHK wind value is 8.087kW (average wind speed of 11.41m/s); in contrast, using OOST formulations leads to a power of 7.207 kW (average wind speed of 10.98m/s). Intermediate values are obtained for T—Y and DREN formulations: 7.365kW and 7.346kW, respectively. The cubic relationship between wind power and wind velocity highlights the importance of accurate estimations of wind intensity for wind energy resources using coupling techniques (a maximum percentage of 10% is assessed). This example shows the relevance of coupled effects for an accurate wind power assessment for wind farm project plans.

The wave-limited fetches and the persistency of offshore winds represent particular ocean—atmosphere conditions never investigated before from a full-coupling perspective; only energetic cyclogenesis activity has been recently modelled and investigated (e.g. Warner et al., 2010, Olabarrieta et al., 2012; Zambon et al., 2014; Renault et al., 2012) where also the heat transfer plays a relevant role in the air—sea coupling. In the mentioned cases, extreme modelled waves and wind benefitted from the use of full-coupling systems. Our case presents less energetic conditions; however the cubic relationship between the potential wind energy and the wind intensity may justify for engineering purposes the use of coupled formulations between wind and waves. Further observational campaigns and the future use of high-resolution remote-sensing products (e.g. Sentinel-1 and Sentinel-3; Torres et al., 2012 and Malenovsky et al., 2012) will benefit the numerical results and extended physical investigations in such a complex process as wind jet, in particular the role of the air—sea transfer formulations. Our results are also relevant in that they may be useful for further physical investigations in similar domains where the wind jets control the ocean—atmosphere dynamics (Jiang et al., 2009; Barton et al., 2009; Shimada and Kawamura, 2006).

5 Conclusions

Wind jet events, investigated using numerical modelling and both in situ and remote-sensing data, present particular conditions in meteo-oceanographic variables in the northern margin of the Ebro delta. A fully coupled meteo-oceanographic numerical model was implemented, with a good level of agreement in terms of waves, currents and wind fields measured. The numerical results reveal a spatially varying wind pattern, forming a well-limited wind jet. The water current velocity pattern during wind jet is well correlated with the wind intensities in the surface layer. However, in deep layers the flow becomes complex, and other processes of larger temporal and spatial characteristic scales affect the water circulation. The wave modelling during the wind jet events is characterized by the developing of bimodal wave spectra: local wave generation due to wind jet and waves propagated from the open sea. Numerical results from sensitivity tests have shown the relatively small relevance of air—sea transfer formulations considering the significant wave height for the sea bottom roughness estimation. Furthermore, the accurate estimation of the wind energy resource may be benefitted by the coupled numerical modelling. The characteristics of the meteo-ocean variables during the wind jet in the northern Ebro delta may be useful for understanding processes in similar domains under severe cross-shelf wind conditions.

Nonlin. Processes Geophys. Discuss., doi:10.5194/npg-2016-8, 2016
Manuscript under review for journal Nonlin. Processes Geophys.
Published: 25 January 2016

Nonlinear Processes in Geophysics
Discussions
Open Access

Appendix 1. Modification of the whitecapping term in SWAN

Pallarès et al. (2014) performed numerical experiments that aimed to improve the numerical wave predictions in semi-enclosed bays, modifying the dissipation terms in the wave energy balance equation. For this purpose two whitecapping formulations are considered in SWAN, obtained from the pulse-based model of Hasselmann (1974) reformulated in terms of wave number (the WAMDI group, 1988):

$$S_{ds,w}(\sigma,\theta) = -\Gamma\tilde{\sigma}\frac{k}{\tilde{k}}E(\sigma,\theta) \quad , \qquad \text{(A1.1)}$$

where $\tilde{\sigma}$ and $\tilde{k}$ denote the mean frequency and the mean wave number, respectively, and the coefficient Γ depends on the wave steepness (Janssen 1991):

$$\Gamma = C_{ds}\left((1-\delta)+\delta\frac{k}{\tilde{k}}\right)\left(\frac{\tilde{s}}{\tilde{s}_{PM}}\right)^{p} \quad . \qquad \text{(A1.2)}$$

The coefficients C_{ds}, δ and p can be adapted to the study case; $\tilde{s}$ is the overall wave steepness; and $\tilde{s}_{PM}$ is the value of $\tilde{s}$ for the Pierson—Moskowitz spectrum (1964).

In SWAN the previously mentioned coefficients are obtained by adjusting the energy balance for idealized wave growth conditions (fully developed wind seas in deep water), despite the wave growth in semi-enclosed domains with highly variable wind fields differing considerably from those idealized conditions. As a result of a calibration process in the NW Mediterranean Sea, which led to a reduction of the wave forecast errors mainly present in the wave period, the coefficients selected for the wind jet region were δ=1 , C_{ds} = 2.36x10^{-5} and p=4, achieving a notable fit between numerical outputs and wave observations.

Appendix 2. Air—sea momentum transfer formulations (bottom roughness length)

The standard bottom roughness length scale is expressed as a function of the Charnok coefficient (Ca; typical value of 0.016 for rapidly sees) and surface wind stress (u_s):

$$z_0=C_a \cdot u_s^2/g \quad , \qquad \text{(A2.1)}$$

Nonlin. Processes Geophys. Discuss., doi:10.5194/npg-2016-8, 2016
Manuscript under review for journal Nonlin. Processes Geophys.
Published: 25 January 2016

Nonlinear Processes in Geophysics Discussions Open Access EGU

where g is the gravity. Coupling online simulations in COAWST allows three different formulations to be chosen to parameterize the bottom roughness considering the wave effects. The formulation of Taylor and Yelland (2001) considers the wave effects:

$$z_0=1200\cdot(H_S/L_p)^{4.5} \quad , \qquad \text{(A2.2)}$$

where Hs is the significant wave height and L_P is the wavelength at the peak of the wave spectrum. Drennan et al. (2003) proposed a formulation to estimate z_0 as a function of the phase-wave speed (C_p) and wind friction velocity (u*):

$$z_0=3.35\cdot(u^*/C_p)^{3.4} \qquad \text{(A2.3)}$$

Similar to Drennan's formulation, Oost et al. (2002) proposed the following formulation based on an experimental data set:

$$z_0=25.0/\pi\cdot(u^*/C_p)^{4.5} \quad . \qquad \text{(A2.4)}$$

Conceptual differences arise from these formulations: Taylor and Yelland (2001) considers the wave steepness, Drennan et al. (2003) is based on the wave age and Oost et al. (2002) considers effects of both wave steepness and wave age.

Acknowledgements

The authors are thankful to Joan Puigdefàbregas (LIM/UPC, Barcelona), Joaquim Sospedra (LIM/UPC, Barcelona) and Jordi Cateura (LIM/UPC, Barcelona) for the data acquisition. The research leading to these results and data acquisition received funding from Mestral (CTM-2011-30489), Neptune (KIC project 006-2012-R01-IREC-OFF-AERO), Hareamar/Dardo (ENE2012-38772-C02-02), Rises-AM (GA603396), Plan-Wave (CTM2013-45141-R) and the iCOAST project (ECHO/SUB/2013/661009).

References

Alomar, M., A., Sánchez-Arcilla, R. Bolaños, and A. Sairouni (2014), Wave growth and forecasting in variable, semi-enclosed domains, *Cont. Shelf Res.*, *87*, 28–40, doi:10.1016/j.csr.2014.05.008.

Barton, E. D., M. F. Lavín, and A. Trasviña (2009), Coastal circulation and hydrography in the Gulf of Tehuantepec, Mexico, during winter, *Cont. Shelf Res.*, *29*(2), 485–500, doi:10.1016/j.csr.2008.12.003.

Bolaños-Sanchez, R., A. Sanchez-Arcilla, and J. Cateura (2007), Evaluation of two atmospheric models for wind–wave modelling in the NW Mediterranean, *J. Mar. Syst.*, *65*(1-4), 336–353, doi:10.1016/j.jmarsys.2005.09.014.

Booij, N., R. C. Ris, and L. H. Holthuijsen (1999), A third-generation wave model for coastal regions: 1. Model description and validation, *J. Geophys. Res.*, *104*(C4), 7649, doi:10.1029/98JC02622.

Cerralbo, P., M. Grifoll, J. Moré, M. Bravo, A. Sairouní Afif, and M. Espino (2015), Wind variability in a coastal area (Alfacs Bay, Ebro River delta), *Adv. Sci. Res.*, *12*, 11–21, doi:10.5194/asr-12-11-2015.

Csanady, G. T. (1980), Longshore pressure gradients caused by offshore wind, *J. Geophys. Res.*, *85*(C2), 1076, doi:10.1029/JC085iC02p01076.

Csanady, G. T. (1982), Circultion in the coastal ocean, *Adva. Geophys.*, 23, 101-183.

Drennan, W. M., H. C. Graber, D. Hauser, and C. Quentin (2003), On the wave age dependence of wind stress over pure wind seas, *J. Geophys. Res.*, *108*(C3), 8062, doi:10.1029/2000JC000715.

Drews, C. (2013), Using wind setdown and storm surge on Lake Erie to calibrate the air-sea drag coefficient., *PLoS One*, *8*(8), e72510, doi:10.1371/journal.pone.0072510.

Durand, N., A. Fiandrino, P. Fraunié, S. Ouillon, P. Forget, and J. J. Naudin (2002), Suspended matter dispersion in the Ebro ROFI: an integrated approach, *Cont. Shelf Res.*, *22*(2), 267–284, doi:10.1016/S0278-4343(01)00057-7.

Dzwonkowski, B., K. Park, and L. Jiang (2011), Subtidal across-shelf velocity structure and surface transport effectiveness on the Alabama shelf of the northeastern Gulf of Mexico, *J. Geophys. Res.*, *116*(C10), C10012, doi:10.1029/2011JC007188.

Fewings, M., S. J. Lentz, and J. Fredericks (2008), Observations of Cross-Shelf Flow Driven by Cross-Shelf Winds on the Inner Continental Shelf, *J. Phys. Oceanogr.*, *38*(11), 2358–2378, doi:10.1175/2008JPO3990.1.

Font, J. (1990), A Comparison of Seasonal Winds With Currents on the Continental Slope of the Catalan Sea (Northwestern Mediterranean), *J. Geophys. Res.*, *95*(C2), 1537–1545,

Nonlin. Processes Geophys. Discuss., doi:10.5194/npg-2016-8, 2016
Manuscript under review for journal Nonlin. Processes Geophys.
Published: 25 January 2016

doi:10.1029/JC095iC02p01537.

Grifoll, M., A. L. Aretxabaleta, J. L. Pelegrí, M. Espino, J. C. Warner, and A. Sánchez-Arcilla (2013), Seasonal circulation over the Catalan inner-shelf (northwest Mediterranean Sea), *J. Geophys. Res. Ocean.*, *118*(10), 5844–5857, doi:10.1002/jgrc.20403.

Horwitz, R., and S. J. Lentz (2014), Inner-Shelf Response to Cross-Shelf Wind Stress: The Importance of the Cross-Shelf Density Gradient in an Idealized Numerical Model and Field Observations, *J. Phys. Oceanogr.*, *44*(1), 86–103, doi:10.1175/JPO-D-13-075.1.

Jacob, R., J, Larson and E. Ong (2005) M x N communication and parallel interpolation in CCSM using the Model Coupling Toolkit. Preprints, Mathematics and Computer Science Division, Argonne National Laboratory, Argonne, IL.

Jansà, A. (1985). The “Mistral-Tramuntana” shear line. A satellite observation. Scientific results of the alpine experiment (ALPEX). Grap publications series, 27, Volume II, 577-591.

Janssen, P. (1989), Wave-induced stress and the drag of air flow over sea waves, *J. Phys. Oceanogr.*, *19*, 745–754.

Janssen, P., and P. Viterbo (1996), Ocean waves and the atmospheric climate, *J. Clim.*, *9*, 1269–1287.

Jiang, H., J. T. Farrar, R. C. Beardsley, R. Chen, and C. Chen (2009), Zonal surface wind jets across the Red Sea due to mountain gap forcing along both sides of the Red Sea, *Geophys. Res. Lett.*, *36*(19), L19605, doi:10.1029/2009GL040008.

Jones, P. (1999), First-and second-order conservative remapping schemes for grids in spherical coordinates, *Mon. Weather Rev.*, (3), 2204–2210.

Jordà, G. (2005), Towards data assimilation in the Catalan continental shelf. From data analysis to optimization methods, PhD thesis, Univ. Politècnica de Catalunya, Barcelona, Spain.

Klaić, Z. B., Z. Pasarić, G. Beg Paklar, and P. Oddo (2011), Coastal sea responses to atmospheric forcings at two different resolutions, *Ocean Sci.*, *7*(4), 521–532, doi:10.5194/os-7-521-2011.

Lionello, P., P. Malaguzzi, and A. Buzzi (1998), Coupling between the Atmospheric Circulation and the Ocean Wave Field: an idealized case., , (1), 161–177.

Martín-Vide, J. and J. Olcina, J. (2001). Climas y Tiempos de España, Alianza editorial, Madrid, Spain. 264 pag. In spanish.

Mestres, M., J. P. Sierra, A. Sánchez-arcilla, J. González, Del Río, T. Wolf, and A. Rodríguez (2003), Modelling of the Ebro River plume . Validation with field observations , *67*(4), 379–391.

Nelson, J. and R. He (2012), Effect of the Gulf stream on winter extratropical cyclone outbreaks. Atmos Sci Lett 13:311–316. doi:10.1002/asl.400

Nunalee, C., and S. Basu (2014), Mesoscale modeling of coastal low level jets: implications for offshore wind resource estimation, *Wind Energy*, doi:10.1002/we.

Oddo, P., A. Bonaduce, N. Pinardi, and A. Guarnieri (2014), Sensitivity of the Mediterranean sea level to atmospheric pressure and free surface elevation numerical formulation in NEMO, *Geosci. Model Dev.*, *7*(6), 3001–3015, doi:10.5194/gmd-7-3001-2014.

Olabarrieta, M., J. C. Warner, B. Armstrong, J. B. Zambon, and R. He (2012), Ocean–atmosphere dynamics during Hurricane Ida and Nor'Ida: An application of the coupled ocean–atmosphere–wave–sediment transport (COAWST) modeling system, *Ocean Model.*, *43-44*, 112–137, doi:10.1016/j.ocemod.2011.12.008.

Oost, W. A., G. J. Komen, C. M. J. Jacobs, and C. van Oort (2002), New evidence for a relation between wind stress and wave age from measurements during ASGAMAGE, *Bound. Layer Meterologhy …*, *103*, 409–438.

Palanques, A., P. Puig, and J. Guillén (2002), Near-bottom suspended sediment fluxes on the microtidal low-energy Ebro continental shelf (NW Mediterranean), *Cont. Shelf …*, *22*, 285–303.

Redondo, J. M., A. Matulka, A. Platonov, E. Sekula, and P. Fraunie (2013), Eddy measurements, coastal turbulence and statistics in the gulf of Lions, *Ocean Sci. Discuss.*, *10*(1), 55–81, doi:10.5194/osd-10-55-2013.

Renault, L., J. Chiggiato, J. C. Warner, M. Gomez, G. Vizoso, and J. Tintoré (2012), Coupled atmosphere-ocean-wave simulations of a storm event over the Gulf of Lion and Balearic Sea, *J. Geophys. Res. Ocean.*, *117*(C9), n/a–n/a, doi:10.1029/2012JC007924.

Riosalido, L., Vazquez, A., A. Gordo, A. and A., Jansà (1985). "Cierzo": nortwesterly wind along the Ebro Valley as a meso-scale effect induced on the lee of the Pyrennes mountain range; a case study during alpex special observing period. Scientific results of the alpine experiment (ALPEX). Grap publications series, 27, Volume II, 565-575.

Salat, J. et al. (2002), Seasonal changes of water mass structure and shelf slope exchanges at the Ebro Shelf (NW Mediterranean), *Cont. Shelf Res.*, *22*, 327–348.

Sánchez-Arcilla, A., D. González-Marco, and R. Bolaños (2008), A review of wave climate and prediction along the Spanish Mediterranean coast, *Nat. Hazards Earth Syst. Sci.*, *8*(6), 1217–1228, doi:10.5194/nhess-8-1217-2008.

Schaeffer, A., P. Garreau, A. Molcard, P. Fraunié, and Y. Seity (2011), Influence of high-resolution wind forcing on hydrodynamic modeling of the Gulf of Lions, *Ocean Dyn.*, *61*(11), 1823–1844, doi:10.1007/s10236-011-0442-3.

Shimada, T., and H. Kawamura (2006), Wind-wave development under alternating wind jets and wakes induced by orographic effects, *Geophys. Res. Lett.*, *33*(2), L02602, doi:10.1029/2005GL025241.

Skamarock, W.C., Klemp, J.B., Dudhia, J., Gill, D.O., Barker, D.M., Wang, W., Powers, J.G., (2005). A Description of the Advanced Research WRF, Version 2, NCAR Technical Note, NCAR/TN-468+STR.

Spanish Ministry of Energy (2014), Wind Atlas of Spain; www.mineturb.gov.es

Taylor, P., and M. Yelland (2001), The dependence of sea surface roughness on the height and steepness of the waves, *J. Phys. Oceanogr.*, (1996), 572–590.

Tonani M., A. Teruzzi, G. Korres, N. Pinardi, A. Crise, M. Adani, P. Oddo, S. Dobricic, C. Fratianni, M. Drudi, S. Salon, A. Grandi, G. Girardi, V. Lyubartsev and S. Marino, 2014. The Mediterranean Monitoring and Forecasting Centre, a component of the MyOcean system. Proceedings of the Sixth International Conference on EuroGOOS 4-6 October 2011, Sopot, Poland. Edited by H. Dahlin, N.C. Fleming and S. E. Petersson. First published 2014. Eurogoos Publication no. 30. ISBN 978-91-974828-9-9.

Umlauf, L., and H. Burchard (2003), A generic length-scale equation for geophysical, *J. Mar. Res.*, *61*(2), 235–265, doi:10.1357/002224003322005087.

Warner, J. C., B. Armstrong, R. He, and J. B. Zambon (2010), Development of a Coupled Ocean–Atmosphere–Wave–Sediment Transport (COAWST) Modeling System, *Ocean Model.*, *35*(3), 230–244, doi:10.1016/j.ocemod.2010.07.010.

Zambon, J. B., R. He, and J. C. Warner (2014), Investigation of hurricane Ivan using the coupled ocean–atmosphere–wave–sediment transport (COAWST) model, *Ocean Dyn.*, *64*(11), 1535–1554, doi:10.1007/s10236-014-0777-7.

Zhai, P., and A. Bower (2013), The response of the Red Sea to a strong wind jet near the Tokar Gap in summer, *J. Geophys. Res. Ocean.*, *118*(1), 421–434, doi:10.1029/2012JC008444.

Nonlin. Processes Geophys. Discuss., doi:10.5194/npg-2016-8, 2016
Manuscript under review for journal Nonlin. Processes Geophys.
Published: 25 January 2016

Nonlinear Processes in Geophysics
Open Access
Discussions

Table 1. Resolution (in km) of the different domains/meshes used in the nested system as a function of each model and regional scale. In parentheses the mesh name shown in Figure 1 is shown.

Model	NW Mediterranean	Catalan—Balearic Sea	Catalan coast	Ebro delta
WRF	27 (M1)	9 (M2)	3 (M3)	1 (M4)
SWAN	9 (O1)	3 (O2)	1 (O3)	¼ (O4)
ROMS	-	-	1 (O3)	¼ (O4)

Nonlin. Processes Geophys. Discuss., doi:10.5194/npg-2016-8, 2016
Manuscript under review for journal Nonlin. Processes Geophys.
Published: 25 January 2016

Nonlinear Processes in Geophysics
Discussions

Table 2. Statistics for the comparison between buoy measurements and model outputs. W is the wind intensity (in m·s^{-1}), Hs is the significant waves height (in m), Tm_{01} is the mean wave period (in s) and U and V are the depth-averaged along- and cross-shelf currents, respectively (in cm·s^{-1}). The statistical parameters are the root mean square error (RMSE), the bias and the correlation coefficient (R).

	Observed		RMSE	Bias	R
	Mean	Standard deviation			
W	6.59	4.52	2.70	0.68	0.79
Hs	0.62	0.42	0.29	0.09	0.76
Tm_{01}	3.48	0.92	3.57	1.14	0.57
U	-4.60	3.90	3.07	2.14	0.82

Nonlin. Processes Geophys. Discuss., doi:10.5194/npg-2016-8, 2016
Manuscript under review for journal Nonlin. Processes Geophys.
Published: 25 January 2016

Nonlinear Processes in Geophysics
Discussions
Open Access

Table 3. Statistics for the comparison between buoy measurements and model outputs. W is the wind intensity (in m·s^{-1}); Hs is the significant waves height (in m). Statistics are only for the wind jet event.

		Mean obs/mod	Standard deviation obs/mod	RMSE	R
CHK	W	10.93/11.48	5.65/5.19	4.75	0.62
	Hs	0.74/0.73	0.27/0.32	0.25	0.61
T-Y	W	10.93/11.51	5.65/5.24	4.83	0.61
	Hs	0.74/0.72	0.27/0.31	0.26	0.61
DRE	W	10.93/11.46	5.65/5.24	4.79	0.61
	Hs	0.74/0.72	0.27/0.31	0.26	0.62
OOST	W	10.93/11.47	5.65/5.22	4.85	0.60
	Hs	0.74/0.72	0.27/0.31	0.26	0.61

Nonlin. Processes Geophys. Discuss., doi:10.5194/npg-2016-8, 2016
Manuscript under review for journal Nonlin. Processes Geophys.
Published: 25 January 2016

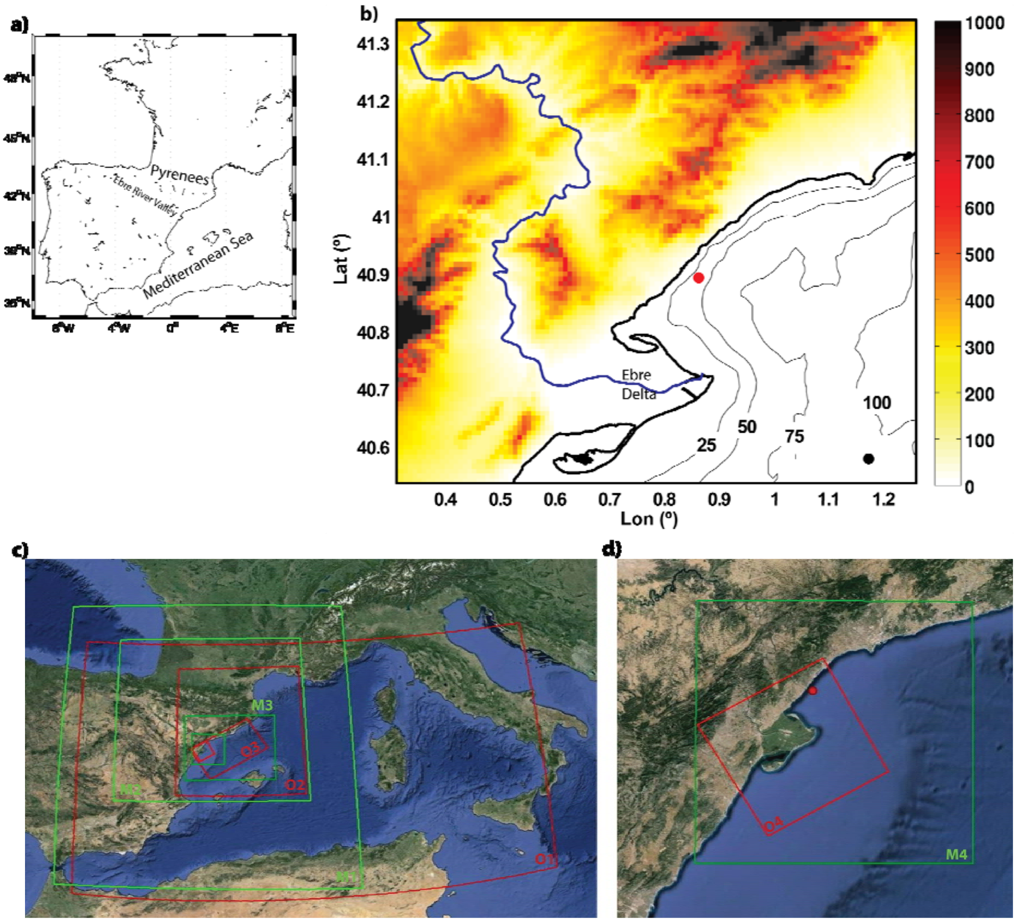

Figure 1. Localization map (a) and orography (coloured map) and bathymetry of the study area (b). The bathymetry lines are shown every 25m. The geographical position where the observational buoy was moored is shown with a red circle. The control point used in the analysis is shown with a black circle. (c, d) Geographical domains for the meteorological model (in green) and the wave and the water circulation model (in red).The mesh notation is also shown (its resolution is detailed in Table 1).

Nonlin. Processes Geophys. Discuss., doi:10.5194/npg-2016-8, 2016
Manuscript under review for journal Nonlin. Processes Geophys.
Published: 25 January 2016

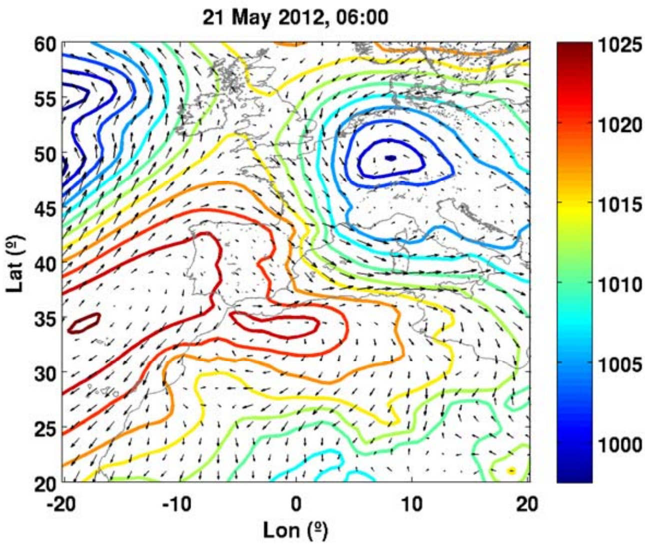

Figure 2. Regional chart of the mean sea level pressure (HPa) during the 21st of May at 06:00 UTC (representative of the synoptic situation during the selected cross-shelf wind event). Data source: ERA-Interim global reanalysis from ECMWF. Arrows represent the wind field.

Nonlin. Processes Geophys. Discuss., doi:10.5194/npg-2016-8, 2016
Manuscript under review for journal Nonlin. Processes Geophys.
Published: 25 January 2016

Nonlinear Processes in Geophysics
Discussions
Open Access

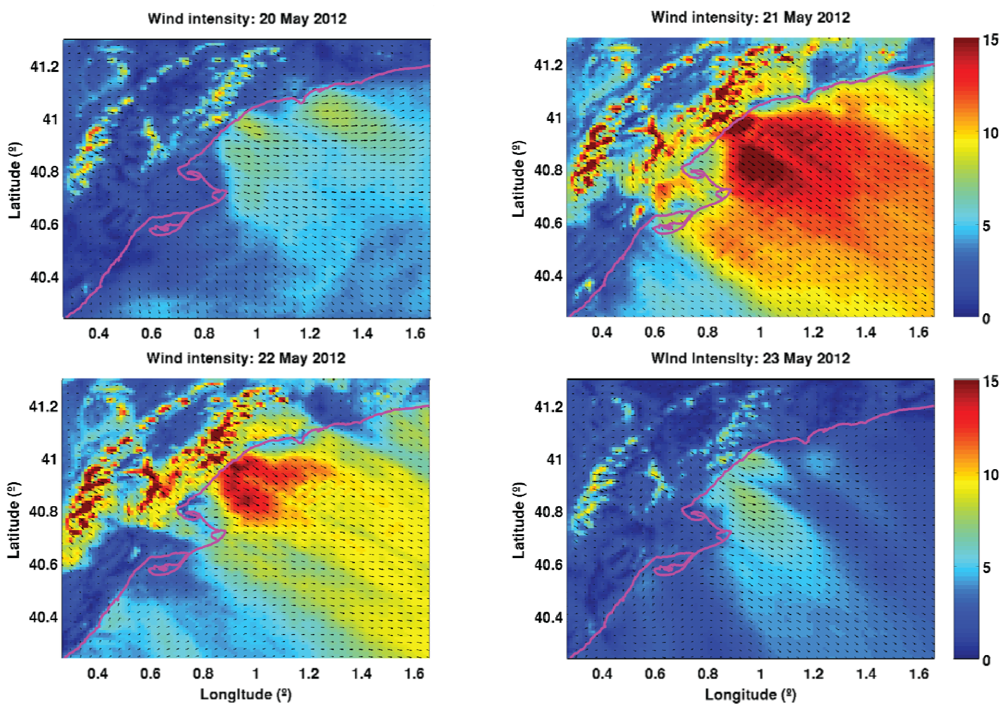

Figure 3. Sequence of the wind jet intensity on four days for a wind jet event in the domain of the Catalan coast. The quiver is shown each three points. COAWST represents the results obtained for the modelling at mesh M3.

Nonlin. Processes Geophys. Discuss., doi:10.5194/npg-2016-8, 2016
Manuscript under review for journal Nonlin. Processes Geophys.
Published: 25 January 2016

Nonlinear Processes in Geophysics
Open Access
Discussions

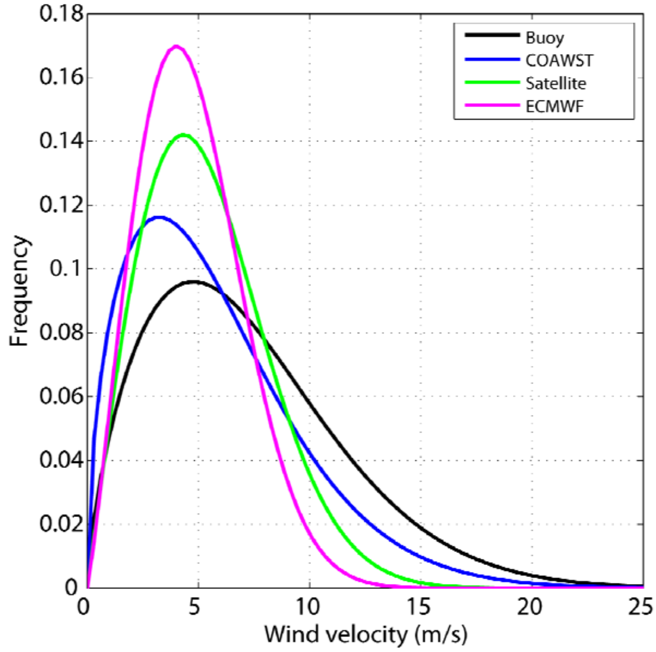

Figure 4. Weibull distribution adjustment for the wind velocities regarding the duration for the 12 months analysed.

Nonlin. Processes Geophys. Discuss., doi:10.5194/npg-2016-8, 2016
Manuscript under review for journal Nonlin. Processes Geophys.
Published: 25 January 2016

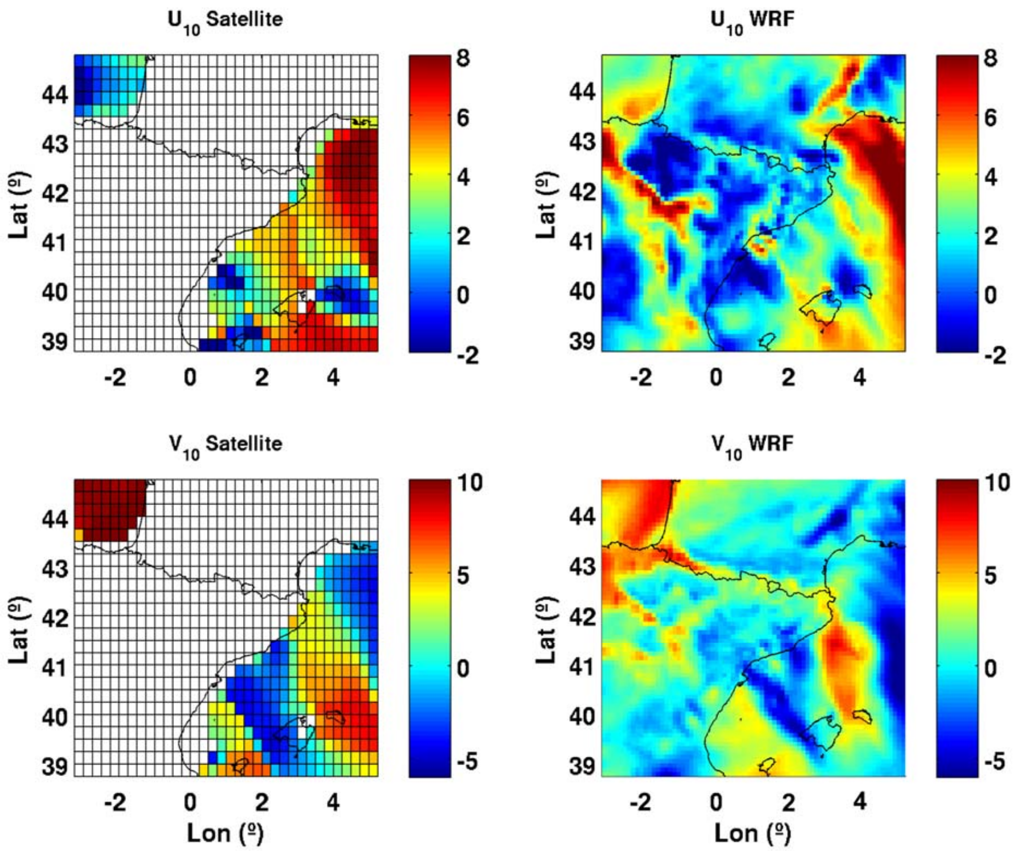

Figure 5. Wind components (top: east—west top; bottom: north—south) from the satellite gridded product for the study area (top) and from the results of the meteorological model. The figure corresponds to 01/01/2012 at 12:00 UTC.

Nonlin. Processes Geophys. Discuss., doi:10.5194/npg-2016-8, 2016
Manuscript under review for journal Nonlin. Processes Geophys.
Published: 25 January 2016

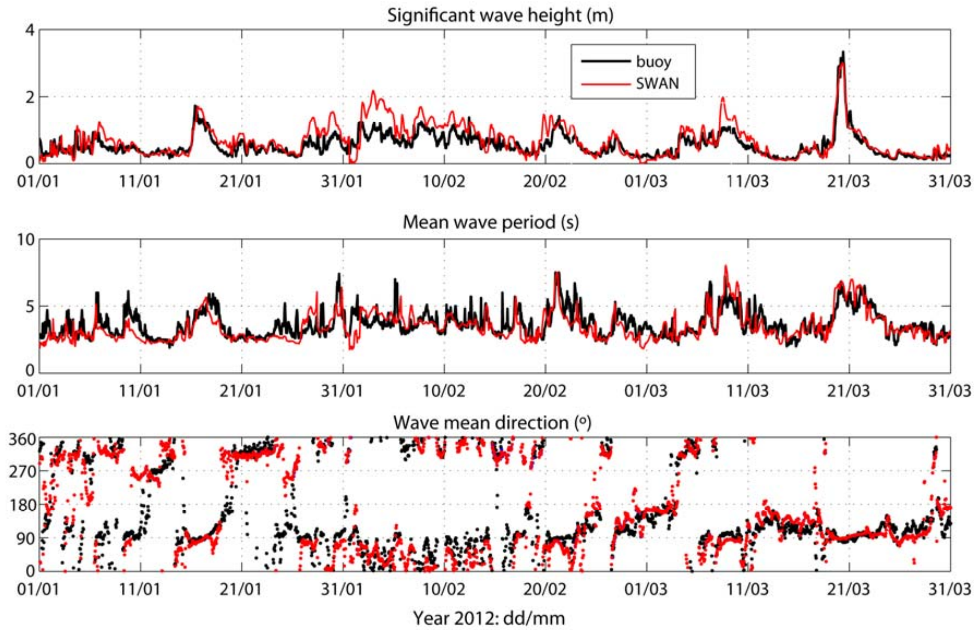

Figure 6. Time series of the significant wave height (m), the mean wave period Tm_{01} (s) and the mean wave direction for the first trimester of 2012. In black the buoy measurement is represented, in blue the results of the non-coupled SWAN model in the buoy location and in red the results of the coupled system.

1 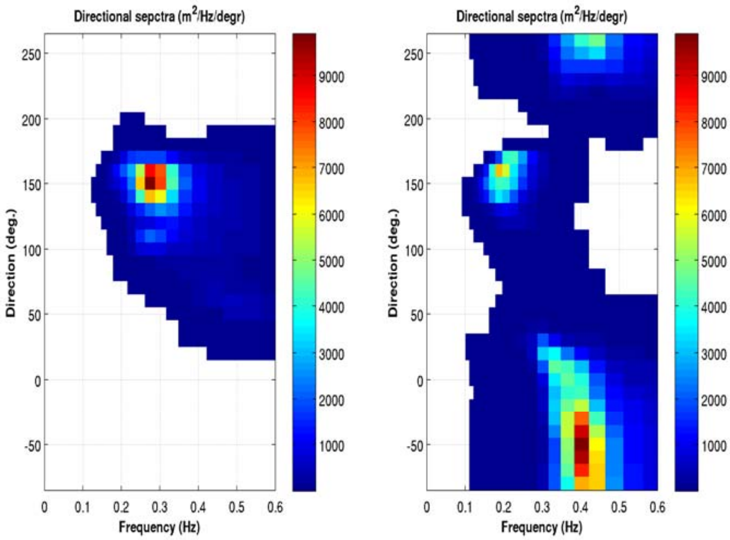

2 Figure 7. Numerical wave spectra for two different instants at the observational point: the
3 wind jet event (left; 5 March 2012) and without wind jet (right; 21 March 2012).

Nonlin. Processes Geophys. Discuss., doi:10.5194/npg-2016-8, 2016
Manuscript under review for journal Nonlin. Processes Geophys.
Published: 25 January 2016

Nonlinear Processes in Geophysics
Discussions
Open Access

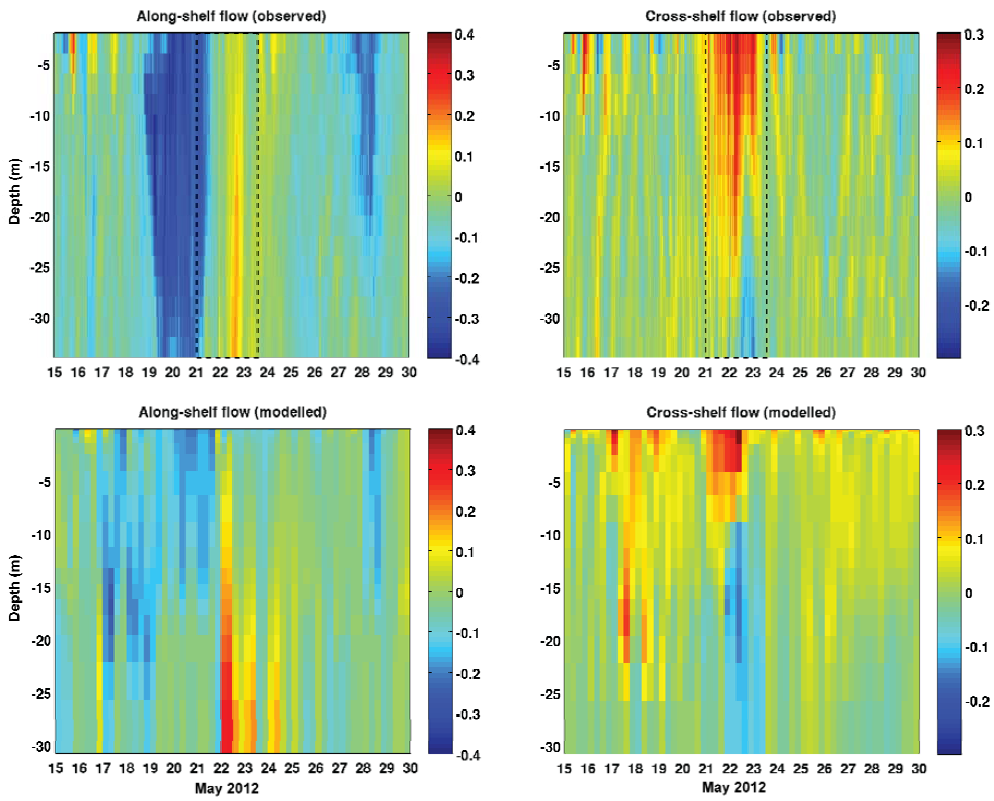

Figure 8. Along-shelf (left) and cross-shelf (right) velocity measured and modelled during May 2012. The wind jet period is marked as a dashed square in the observed values. Note the different velocity ranges between cross-shelf and along-shelf plots.

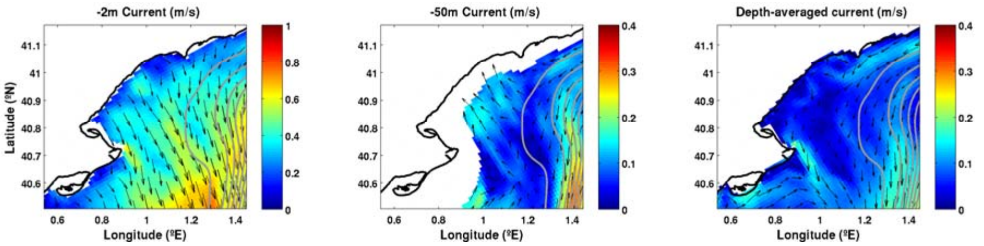

Figure 9. Modelled circulation at -2m (left), -50m (centre) and depth-averaged circulation (right) during the peak of the wind jet event (i.e. 21st of May 2012, 06:00 UTC). The quiver is shown each four computational points. Grey lines are shown each 100 isobaths. Note differences in the velocity ranges among the sub-plots.

Nonlin. Processes Geophys. Discuss., doi:10.5194/npg-2016-8, 2016
Manuscript under review for journal Nonlin. Processes Geophys.
Published: 25 January 2016

1 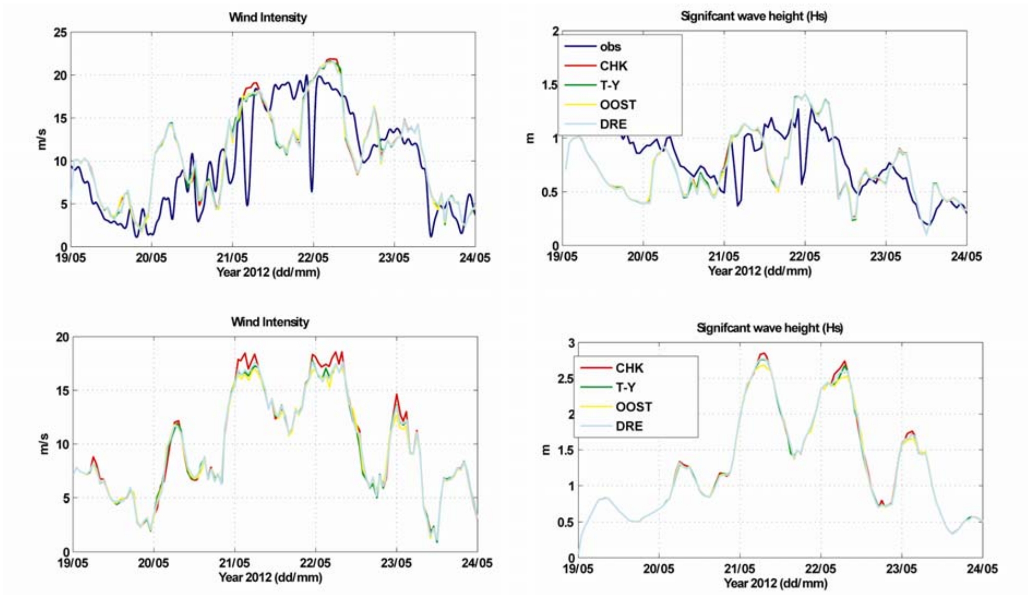

2 Figure 10. Wind intensity (left) and significant wave height (right) for the wind jet energetic
3 event for the observational (top) and control (bottom) points.

Nonlin. Processes Geophys. Discuss., doi:10.5194/npg-2016-8, 2016
Manuscript under review for journal Nonlin. Processes Geophys.
Published: 25 January 2016

Nonlinear Processes in Geophysics
Discussions
Open Access

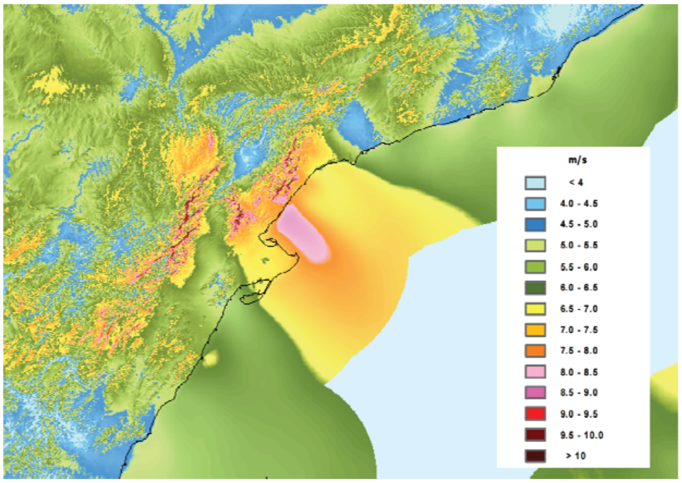

Figure 11. Wind atlas annual mean wind speed at 30m height from a reanalysis product (source: Spanish Ministry of Energy, 2014).